Nano Research 2017, 10(4): 1149–1162
DOI 10.1007/s12274-016-1287-3
Research Article
ISSN 1998-0124
CN 11-5974/O4

One-pot/three-step synthesis of zinc-blende CdSe/CdS core/shell nanocrystals with thick shells

Yuan Niu[§], Chaodan Pu[§], Runchen Lai, Renyang Meng, Wanzhen Lin, Haiyan Qin, and Xiaogang Peng (✉)

Center for Chemistry of Novel and High-Performance Materials, and Department of Chemistry, Zhejiang University, Hangzhou 310027, China

[§] *These authors contributed equally to this work.*

Received: 12 July 2016
Revised: 11 September 2016
Accepted: 12 September 2016

KEYWORDS
zinc-blende,
core/shell,
quantum dots,
thick shells

ABSTRACT

A one-pot/three-step synthetic scheme was developed for phase-pure epitaxy of CdS shells on zinc-blende CdSe nanocrystals to yield shells with up to sixteen monolayers. The key parameters for the epitaxy were identified, including the core nanocrystal concentration, solvent type/composition, quality of the core nanocrystals, epitaxial growth temperature, type/concentration of ligands, and composition of the precursors. Most of these key parameters were not influential when the synthetic goal was thin-shell CdSe/CdS core/shell nanocrystals. The finalized synthetic scheme was reproducible at an almost quantitative level in terms of the crystal structure, shell thickness, and optical properties.

1 Introduction

Development of synthetic approaches [1–3] for generating colloidal semiconductor nanocrystals with sizes in the quantum confinement regime (quantum dots) is a key requirement for fundamental understanding of these species and exploration of their technical applications. Recently, the emphasis in this area has shifted towards synthesis of nanocrystals with complex structures and/or compositions [4–7]. For such synthetic development, core/shell quantum dots [8–14] are the basic model systems. Core/shell quantum dots are almost the only such acceptable species for technical applications as luminescent materials. For example, although CdSe quantum dots with near-unity photoluminescence (PL) quantum yield (QY) and single-exponential PL decay dynamics can be fabricated [15], they are not sufficiently chemically and optically stable to withstand the challenging environments of most applications. Semiconductor shells with valence bands (conduction bands) that are lower (or higher) than that of the core semiconductor can greatly improve the stability of the quantum dots in harsh environments if high quality and homogeneous epitaxy between the shells and single-crystalline core nanocrystals can be achieved.

Address correspondence to xpeng@zju.edu.cn

Not surprisingly, core/shell quantum dots with relatively thick shells are often found to be desirable. The most studied core/shell quantum dots [9, 11–14, 16–18], i.e., CdSe/CdS core/shell quantum dots with more than ~15 monolayers of the CdS shells ("giant quantum dots") having the wurtzite structure, have been widely explored as nearly non-blinking quantum dots since 2008 [16, 17]. PL blinking (of a quantum dot) refers to random switching of the PL intensity of a single quantum dot between different brightness states under constant excitation [19], which is an apparent roadblock for promising applications of quantum dots as luminescent materials. Cadmium chalcogenides, including both CdSe and CdS, can adopt either the zinc-blende (face-center cubic) or wurtzite (hexagonal) crystal structure. In principle, differences in the lattice symmetry would result in different electronic band structures and optical properties of the corresponding quantum dots [15, 20–23]. Control of the phase purity of cadmium chalcogenide nanocrystals has been an interesting fundamental topic [24–26]. However, controlled epitaxial growth of phase-pure CdSe/CdS core/shell quantum dots (as the most studied system) with thick shells is still challenging.

In this study, we systematically evaluate the experimental parameters influencing epitaxial growth of phase-pure CdSe/CdS core/shell quantum dots having the zinc-blende structure in the medium (between 7–11 monolayers of the CdS shells) and thick (>11 monolayers of the CdS shells) shell ranges. The results reveal that epitaxial growth of medium and thick shells is dependent on several newly revealed parameters, some of which are somewhat against conventional wisdom. After identification of these key parameters, synthesis of CdSe/CdS core/shell nanocrystals with a shell thickness of up to sixteen monolayers is performed at an almost quantitative level. The position of the PL peaks, the PL QY, PL peak width, PL decay dynamics, blinking behavior, size (shell thickness), and crystal structure of these species are tightly and reproducibly controlled. The resulting series of CdSe/CdS core/shell quantum dots enable systematic studies of the shell-thickness dependence of a variety of optical properties of the CdSe/CdS core/shell nanocrystals. The entire series of core/shell quantum dots was previously proven to be nearly non-blinking [27], though the synthetic chemistry was not discussed. Furthermore, CdSe/CdS core/shell quantum dots with CdS shells comprising ten monolayers developed via the synthetic approach described herein enabled fabrication of quantum dot light-emitting-diodes with nearly ideal performance [28].

2 Results and discussion

For simplicity, we hereafter refer to 1–6 monolayers of the CdS shells as "thin shell", 7–11 monolayers of the CdS shells as "medium shell", 12–16 monolayers of the CdS shells as "thick shell", and more than 16 monolayers of the CdS shells as "very thick shell". The initial reference point for the thickness was the "giant quantum dots" [16, 17, 29]. In 2012, we reported a successful synthetic scheme for epitaxial growth of up to six monolayers of CdS shells on zinc-blende CdSe nanocrystals using cadmium diethyldithiocarbamate ($Cd(DDTC)_2$) as the single precursor [13]. Though simple extension of this successful scheme beyond six monolayers of the CdS shells failed badly (see below), the basic features of that approach form the basis of this work.

The experimental details are provided in the Experimental section. For convenience, a brief description of the experimental system is as follows. After *in situ* purification using a modified procedure [13], CdSe core nanocrystals with the zinc-blende structure were mixed with fatty amine and dodecane. $Cd(DDTC)_2$ was applied as the single-source precursor for thin-shell synthesis, whereas cadmium alkanoates were added to the precursor solution for the quantum dots having relatively thick shells. According to literature [30], decomposition of each $Cd(DDTC)_2$ molecule under elevated temperatures with fatty amine in solution should efficiently generate one molecule of CdS and H_2S. H_2S must then be eliminated from the solution to obtain core/shell nanocrystals with high PL QY [31]. When cadmium alkanoates are added for growth of the relatively thick shells, H_2S reacts with the cadmium alkanoates during the epitaxial growth [32]. The precursors needed for epitaxy of a targeted monolayer were dissolved in an octane/amine mixture. A thermo-cycling technique [33], involving addition of the precursor solution at low temperature and

increasing the temperature for the epitaxial growth, was applied for each monolayer of epitaxy.

2.1 Colloidal stability of the core/shell nanocrystals during epitaxy: solvents and ligands

Molecular interactions between semiconductor nanocrystal-ligand complexes were reported to increase linearly with the volume of the nanocrystals for a given type of ligand, thereby resulting in a drastic decrease of the solubility of the nanocrystal-ligand complexes in a given organic solvent [34]. This implies that, in comparison with the thin-shell dots, the solubility of the medium- and thick-shell quantum dots in the reaction solution might become an issue. Aggregation of the quantum dots would cause inhomogeneous deposition of the shell materials instead of homogeneous epitaxy on each individual nanocrystal [29].

The same solvent system used previously [13] for synthesis of the thin-shell core/shell quantum dots became visibly turbid when the shell thickness increased to the medium- and thick-shell range. Replacement of octane—the solvent in the existing scheme [13]—by dodecane was found to prevent precipitation of the nanocrystals having less than ~20 monolayers of the CdS shells. The ligands applied for epitaxy were also found to play an important role in maintaining the stability of the nanocrystal colloidal [29]. To grow thick-shell quantum dots, a mixture of oleylamine and octylamine was found to render the necessary solubility, while concentration of the ligands produced limit effects. This was found to be consistent with the concept of entropic ligands reported recently [35].

2.2 Particle concentration and morphology/crystal structure control

The morphology of the CdSe/CdS core/shell quantum dots synthesized using the previous system [13] deviated drastically from dot-shaped in the case of the medium and thick CdS shells (Fig. 1(a)). Similar to the previous report [13], the nanocrystals with six monolayers of the CdS shells were slightly non-spherical. For the medium- and thick-shell nanocrystals, the dots became substantially irregular, branched, and elongated. Simultaneously, wurtzite diffraction features gradually became visible in the X-ray powder diffraction (XRD) patterns of the core/shell dots (Fig. 1(b)).

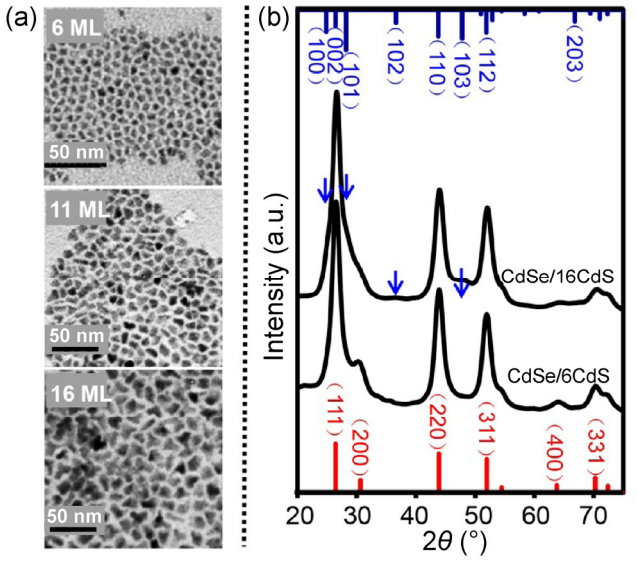

Figure 1 (a) TEM images of CdSe/CdS core/shell nanocrystals with 6 monolayers (6 ML), 11 monolayers (11 ML), and 16 monolayers (16 ML) of CdS. (b) XRD patterns of CdSe/CdS core/shell nanocrystals with 6 ML and 16 ML of CdS shell. The standard diffraction patterns of bulk CdS in either zinc-blende (bottom, red lines) or wurtzite (top, blue lines) form are given as references. The blue arrows indicate minor signals from the wurtzite structure.

The new solution system described above did not completely mitigate the morphological and structural defects of the resulting core/shell nanocrystals with thick shells when the other parameters remained the same (Fig. 2, second row). Previous work suggests that elongation usually occurs with a relatively high monomer concentration and/or high monomer reactivity [2]. Experiments were carried out to decrease the reactivity of the precursors, including decreasing the concentration of the fatty amine (which is the activation reagent for the precursor) [13] and/or the reaction temperature. However, to enable epitaxial growth on the surface of the quantum dots, the reaction temperature cannot be too low. Decreasing the amine concentration could also be problematic as it would induce significant formation of wurtzite defects (discussed below). Furthermore, dividing the precursor solution for a given monolayer into several doses for injection [36]—equivalent to reduction of the precursor concentration—produced limited improvement.

The literature suggests that decreasing the concentration of the nanocrystals may be an effective method to improve the quality of homogeneous epitaxy [37].

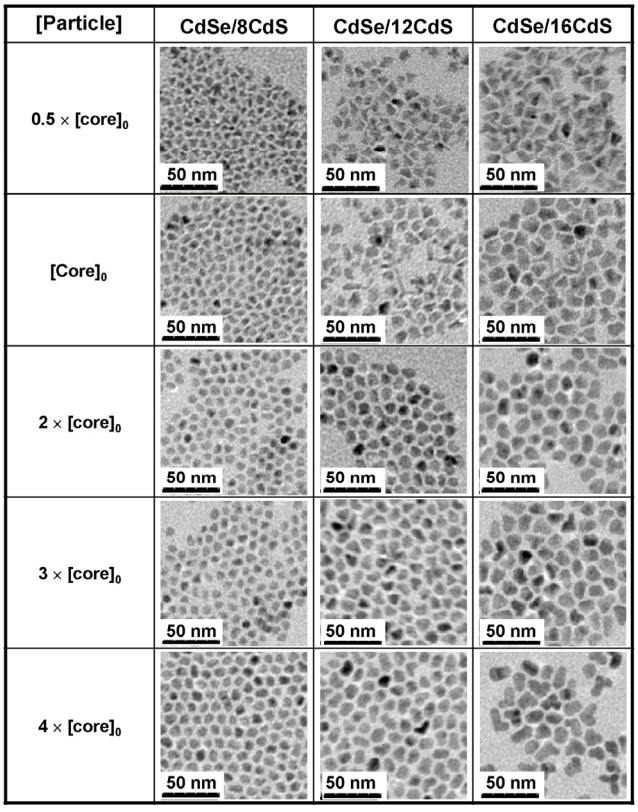

Figure 2 TEM images of CdSe/CdS core/shell nanocrystals with different shell thicknesses, grown with different core nanocrystal concentrations ([particle]). $[Core]_0 = 1.7 \times 10^{-5}$ mol/L.

The initial core nanocrystal concentration—the nanocrystal concentration in the solution prior to addition of any precursor solution—applied previously was 1.7×10^{-5} mol·L^{-1} [13], which was denoted as the original core concentration ($[core]_0$). Experiments were carried out to systematically examine the effects of the nanocrystal concentration by holding the other parameters constant (Fig. 2). For the series of comparative reactions summarized in Fig. 2, growth of the shells proceeded one monolayer at a time regardless of the concentration of the core nanocrystals. This means that the precursor concentration increased in proportion to the concentration of core nanocrystals.

Surprisingly, the morphology of the resulting core/shell nanocrystals with core concentrations below $[core]_0$ became even more irregular than the morphology of those from the reaction with the original core concentration (compare the first two rows in Fig. 2). In contrast, increasing the core concentration to 2 times, 3 times, and 4 times $[core]_0$ significantly improved the morphology and size/shape distribution of the resulting core/shell nanocrystals, as evidenced for the thick-shell nanocrystals (see the last three rows in Fig. 2).

A possible explanation of the unexpected dependence of the size/shape distribution of the core/shell nanocrystals on the core nanocrystal concentration may be the reduction of the diffusion length of the precursors (or active monomers) in the reaction solution by increasing the particle concentration [38]. For growth of core nanocrystals with various compositions, high nanocrystal concentrations greatly promote transfer of the monomers from small nanocrystals to large nanocrystals in solution [2]. Such monomer transfer can be viewed as direct inter-particle diffusion of the monomers, given the overlap of diffusion of the spheres between neighboring nanocrystals under high nanocrystal concentrations. When the nanocrystal concentration is sufficiently high, dissolution of relatively small nanocrystals would be so rapid and complete that the size distribution of the ensemble would be focused—termed as self-focusing [2]. For epitaxial shell growth on the existing nanocrystals in this work, reducing the diffusion length should suppress homogeneous nucleation of the shell materials. Furthermore, if homogeneous nucleation did occur, a high concentration of core nanocrystals would eliminate such tiny CdS nanocrystals rapidly.

If the core concentration was too high, however, the increased chemical potential of the precursors would make growth too fast to be controlled. Figure 2 illustrates that the resulting core/shell nanocrystals with twelve and fourteen monolayers of the CdS shells with the highest core concentration ($4 \times [core]_0$) comprised a high portion of branched nanocrystals. Literature results indicated that the branched structure of II-VI semiconductor nanocrystals usually resulted from growth of wurtzite "arms" from a zinc-blende "body", and required high monomer concentrations [2, 39]. Consistent with this model, the high resolution transmission electron microscopy (HRTEM) images demonstrated the presence of significant wurzite domains in these branches (Fig. S1 in the Electronic Supplementary Material (ESM)). With an even higher core concentration ($6 \times [core]_0$), branched dots dominated

the entire nanocrystal population (Fig. S2 in the ESM).

XRD patterns also verified the core-concentration dependent appearance of wurtzite diffraction features along with the main features of the zinc-blende structure. As demonstrated in Fig. 3, for the CdSe/16CdS core/shell nanocrystals, minor wurtzite diffraction features were identifiable for the reaction employing either the original core concentration or 4 times the original core concentration. Conversely, no wurtzite diffraction features appeared in the XRD patterns for the reactions employing 2 times and 3 times the original core concentration.

2.3 Controlled epitaxy and concentration of fatty amines

The fatty amine plays dual roles in epitaxial growth of CdSe/CdS core/shell nanocrystals, namely, as an activation reagent for $Cd(DDTC)_2$ [30, 33] and as ligands for the nanocrystals. Fatty amines have been identified as relatively weak ligands for cadmium chalcogenide nanocrystals [40], and it would thus be necessary to retain a relatively high concentration in the epitaxial solution. However, a high concentration of fatty amines would over-promote the decomposition of $Cd(DDTC)_2$, thereby inducing self-nucleation of the CdS nanocrystals [30, 33].

The analysis presented above implies that the concentration of fatty amines in the epitaxial solution should have a suitable range. The data in Fig. 4(a)

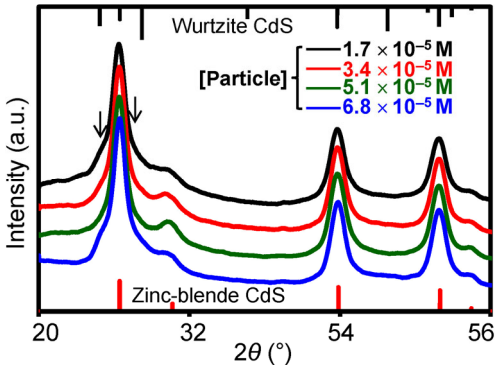

Figure 3 XRD patterns of CdSe/CdS core/shell nanocrystals with 16 ML of the CdS shell, grown with different [particle]. The standard diffraction patterns of bulk CdS in both zinc-blende (bottom, red lines) and wurtzite (top, black lines) form are given as references. The black arrows indicate minor signals from the wurtzite structure.

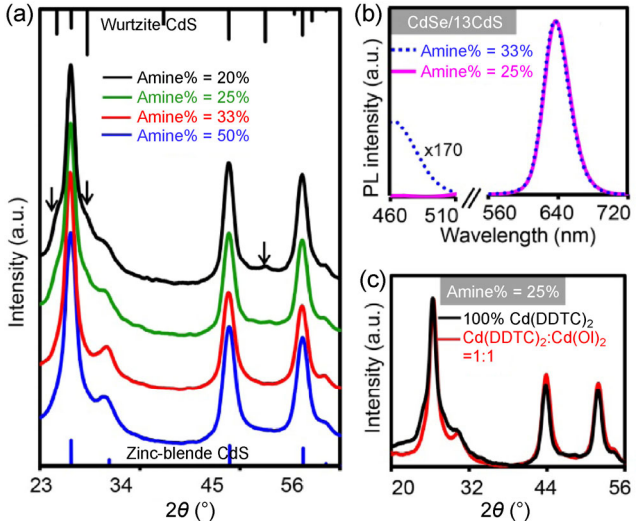

Figure 4 Effects of amine concentration. (a) XRD patterns of CdSe/CdS core/shell nanocrystals with 16 monolayers of CdS shell, grown with different amine concentrations, in units of volume percentage (amine%). The standard diffraction patterns of bulk CdS in both zinc-blende (bottom, red lines) and wurtzite (top, black lines) form are given as references. The black arrows indicate minor signals from the wurtzite structure. (b) PL spectra of CdSe/CdS core/shell nanocrystals with 13 monolayers of CdS shell. (c) XRD patterns of CdSe/CdS core/shell nanocrystals with 16 monolayers of CdS shell, grown with amine concentration of 25% and different $Cd(DDTC)_2/Cd(Ol)_2$ ratios.

confirmed this hypothesis, where the amine concentration was defined as the initial volume percentage of fatty amines in the mixed solvent. Along with the main features of the zinc-blende structure, minor wurtzite diffraction features were observed for reactions employing either high (50%) or low (20%) amine concentrations.

Replacing octylamine with oleylamine of an equimolar concentration could improve the sharpness of the PL peak of the resulting nanocrystals (Fig. S4 in the ESM), but the viscosity of the reaction solution was too high to maintain the necessary colloidal stability for formation of the thick-shell nanocrystals, as mentioned above.

2.4 Balance of colloidal stability and epitaxy by cadmium alkanoates

TEM measurements revealed that the morphology of the thick-shell core/shell nanocrystals for the reaction with 33% amine was still unsatisfactory (Fig. S3 in the ESM).

The dual roles of the fatty amines, i.e., as ligands and activation reagents, could be decoupled by introducing secondary ligands. Cadmium alkanoates are a prospectively good choice, as they are well-known ligands for both CdSe and CdS nanocrystals [41, 42]. According to literature, decomposition of $Cd(DDTC)_2$ generates one molecule each of CdS and H_2S [30, 43]. Cadmium alkanoates could be consumed by the excess H_2S generated by the decomposition of $Cd(DDTC)_2$. Therefore, cadmium alkanoates could also serve as a secondary precursor to somewhat restrict the solution reactivity of $Cd(DDTC)_2$, given their localization on the surface of the nanocrystals as ligands.

Addition of cadmium alkanoates to the reaction frequently caused formation of CdS particles in the late stage of the shell growth for the reactions employing relatively high amine concentrations, as indicated by the new PL peak at high energy positions (see the reaction with 33% amine in Fig. 4(b) as an example). Reducing the amine concentration to 25% suppressed formation of the CdS nanocrystals (Fig. 4(b)). Fortunately, a relatively low amine concentration (25%) and addition of cadmium oleate ($Cd(Ol)_2$) also eliminated the minor wurtzite diffraction features (Fig. 4(c)).

As mentioned above, cadmium alkanoates should be considered as a secondary precursor. The ratio between $Cd(DDTC)_2$ and $Cd(Ol)_2$ may thus be an important parameter during epitaxy. The results presented in Fig. 5 and Fig. S5 (in the ESM) suggest that a one-to-one molar ratio yielded thick-shell nanocrystals with the best thickness control. This was thought to be quite reasonable. Decomposition of $Cd(DDTC)_2$ should generate one molecule of CdS and one molecule of H_2S [22, 32]. Presumably, one molecule of $Cd(Ol)_2$ may react with one molecule of H_2S during epitaxy.

2.5 Effects of free fatty acids

We attempted to eliminate formation of pure CdS nanocrystals by addition of free acid to the reaction system because free fatty acids are known to retard formation of plain CdS nanocrystals [2, 44]. Unfortunately, no improvement was observed based on the PL measurements, and the TEM data actually indicated an opposite trend. When the concentration of oleic acid (HOl) increased to 6 times that of $Cd(Ol)_2$, the size/shape distribution deteriorated (compare the fourth row to the second row in Fig. 5). The results in Fig. 5 (the last row) indicate that in the absence of free oleic acid, the size/shape distribution of the resulting CdSe/16CdS core/shell nanocrystals was significantly better than that from the reaction with a relatively large excess of free oleic acid (the fourth row).

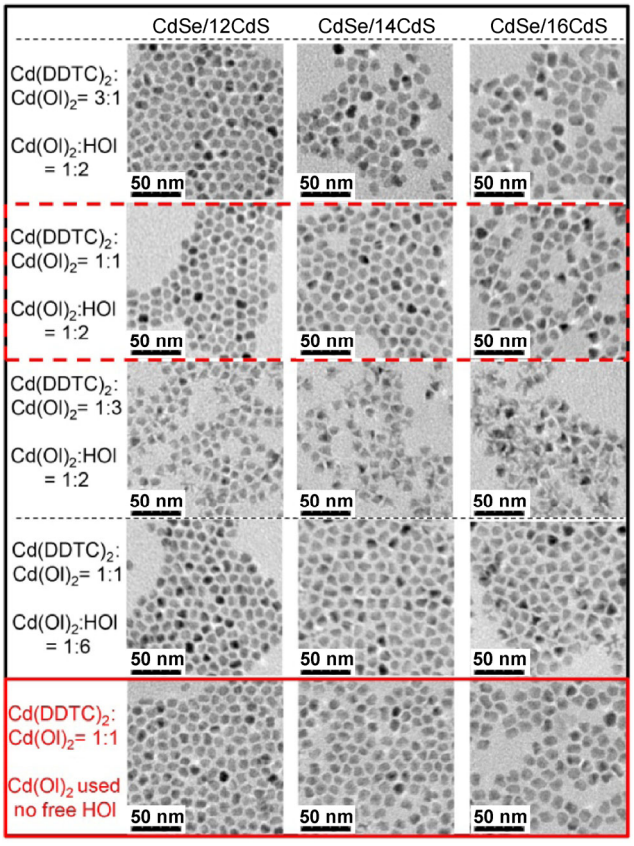

Figure 5 Effects of concentration of Cd fatty acid salts (top three rows) and effects of free acids (bottom two rows).

Furthermore, if the amine concentration was high, the difference between the reactions with and without free acids became substantial (Fig. S6 in the ESM). Based on these results, free fatty acids were excluded for further optimization.

2.6 Quality of core nanocrystals and the resulting core/shell nanocrystals

Previous work revealed that for thin-shell CdSe/CdS core/shell nanocrystals, the PL spectra were often

asymmetric with a tail (or small peak) on the high energy side [13]. This asymmetry was ascribed to the existence of some very small nanocrystals in the core sample synthesized by the so-called non-injection approach [45]. These tiny core particles were not efficiently emissive; however, after shell growth, they became as emissive as the relatively large particles in the same sample. The results in Figs. 6(a) and 6(b) revealed that this problem persisted for the medium- and thick-shell nanocrystals. Furthermore, the position of the high-energy peaks (from ~500 to ~575 nm) in Figs. 6(a) and 6(b) indicated that the asymmetry of the PL spectra must be associated with the CdSe/CdS core/shell nanocrystals with small core sizes, instead of homogeneous nucleation of the CdS nanocrystals.

The non-injection method, in principle, might possess an extended period for nucleation and may form small particles, along with growth of existing particles. This prompted us to improve the situation by applying CdSe core nanocrystals based on a new synthetic strategy developed recently [46], which is based on injection of Se powder suspended in octadecene (Se-SUS) into a hot mixture of cadmium alkanotes and octadecene (see details in the Experimental section). Figure 6(c) shows that application of the core nanocrystals from the Se-SUS approach [46] caused the baselines of the PL spectra to become practically flat on the high energy side and the width of the main PL peak was significantly narrowed (compare Figs. 6(a) and 6(c)).

2.7 General scheme for epitaxy of the CdS shells on CdSe core nanocrystals in zinc-blende structure

The key parameters discussed in the above subsections allowed us optimize the synthetic scheme for formation of zinc-blende CdSe/CdS core/shell nanocrystals with different shell thicknesses. Given the significant differences between the thin-, medium-, and thick-shell dots, a one-pot, three-step strategy (one-pot/three-step) was established (Fig. 7).

The first step was synthesis and *in-situ* purification of the core nanocrystals using the Se-SUS approach [13, 46]. The second step was epitaxial growth of thin-shell dots, i.e., with 1–6 monolayers of the CdS

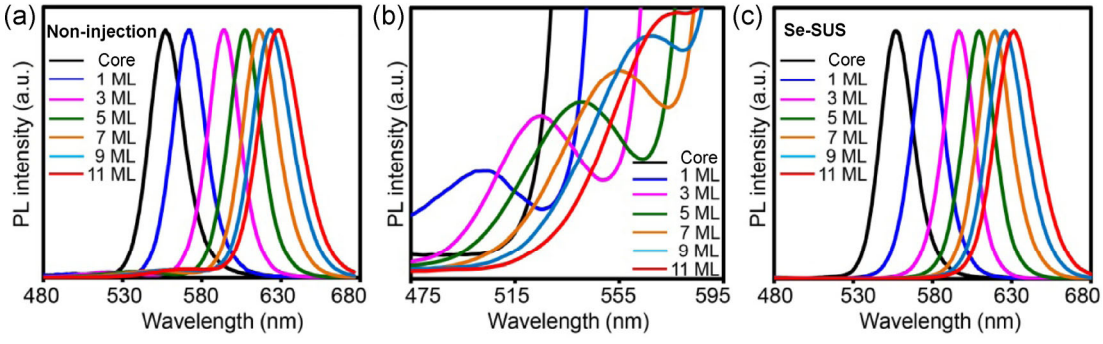

Figure 6 Effects of quality of CdSe core nanocrystals. (a) Evolution of PL spectra of CdSe/CdS core/shell nanocrystals during shell growth using core nanocrystals synthesized by the non-injection approach. (b) Same spectra in (a) but with different *x*- and *y*-axis scales to highlight the small core/shell nanocrystals. (c) Evolution of PL spectra of CdSe/CdS core/shell nanocrystals during shell growth using core nanocrystals synthesized by the Se-SUS approach.

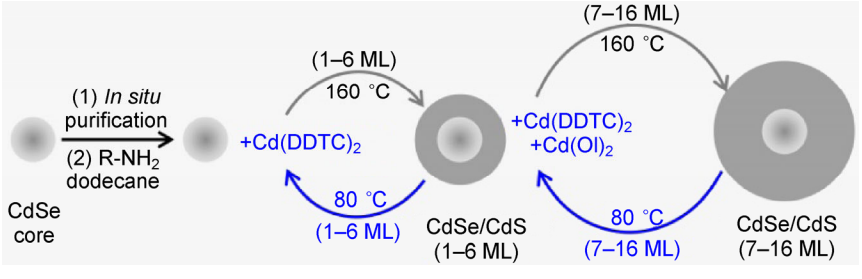

Figure 7 One-pot/three-step synthesis of CdSe/CdS core/shell nanocrystals with zinc-blende structure, having different shell thickness.

shells. In comparison with the previously reported procedure for epitaxy of thin-shell dots [13], the main differences in the second step of the new scheme included changes in the epitaxial growth temperature (~20 ℃ higher than the previous value), the amine concentration (decreased from 55% to 25%), the solvent (replacing octane with dodecane), and the initial concentration of the core nanocrystals (double the value reported previously). These optimizations not only enabled us to reach the synthetic target (CdSe/CdS core/shell nanocrystals with sixteen monolayers of CdS), but also further improved the quality of the CdSe/CdS core/shell nanocrystals with thin-shells (see Fig. 2 and more details below). The main reason for separating the second step from the third step was the need for cadmium alkanoates in the third step.

Figure 8(a) shows the XRD patterns of a core and the corresponding thin-, medium-, and thick-shell dots produced via the optimized scheme (see the Experimental section for details). Upon growth of the CdS shells, the diffraction peaks of the nanocrystals gradually narrowed and shifted from those of the standard CdSe pattern to that of CdS with the pure zinc-blend structure. The shell sizes determined by TEM analysis during growth were plotted along with the theoretical values by assuming a 0.34 nm increase of the shell thickness upon growth of one monolayer of CdS (Fig. 8(b)). The TEM measurements (Fig. 8(c)) revealed that the core/shell nanocrystals with thin- and medium-shell thickness were dot-shaped with excellent size/shape distribution. The thick-shell nanocrystals were nearly dot-shaped with a good size distribution (see more examples in Figs. 5 and 8). Because of the noticeable deviation of the shape from spherical, the shell thickness of the thick-shell species was considered as the average value for the given sample. HRTEM measurements confirmed the single crystalline nature of the zinc-blende CdSe/CdS core/shell nanocrystals with different thicknesses (Fig. 8(c) insets).

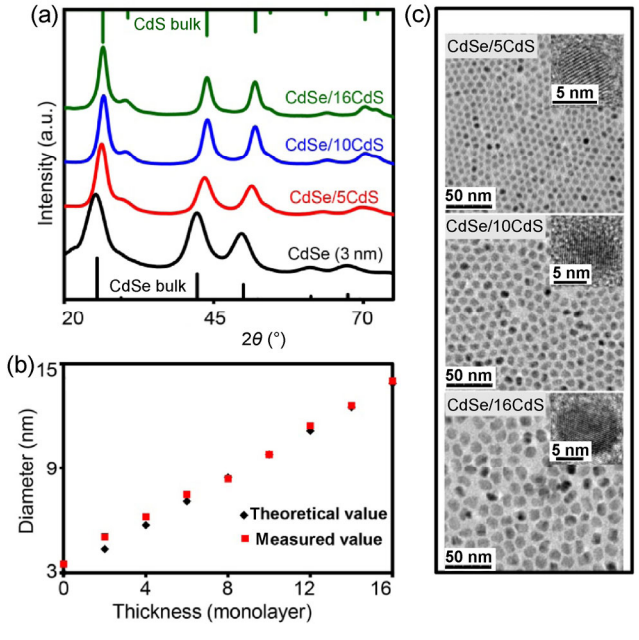

Figure 8 (a) XRD patterns of the CdSe core (first absorption peak at 550 nm) and corresponding core/shell nanocrystals with different shell thickness. (b) Evolution of size of the nanocrystals during shell growth. (c) TEM and HRTEM (insets) images of CdSe/CdS core/shell nanocrystals.

2.8 Shell-thickness dependent optical properties

Figure 9(a) illustrates that upon growth of the CdS shells, the UV–Vis and PL spectra underwent a continuous red-shift. For the series of samples shown in Fig. 9(a), the total shift of the PL peak was very significant, i.e., ~84 nm (from 557 to 641 nm). This substantial and continuous red-shift is consistent with epitaxial growth rather than alloying. Interestingly, although the PL peak shifted monotonically (Fig. 9(a), inset), the PL QY ((Fig. 9(b)), the PL full-width-at-half-maximum (FWHM) (Fig. 9(c)), and the PL decay dynamics (Figs. 9(d) and 9(e)) changed in a drastically different manner.

For the CdSe core nanocrystals in a solution with fatty amines, the absolute PL QY measured by an integrating sphere was ~30%–40%, and the PL decay dynamics of the core nanocrystals was multi-exponential. After growth of two monolayers of the CdS shells, the PL QY of the dots increased to near-unity and the PL decay dynamics of the CdSe/2CdS core/shell QDs became single-exponential with the goodness of fit (χ_R^2) being between 1.0 and 1.3, indicating complete elimination of detrimental traps. These excellent optical features were retained for the nanocrystals with up to ten monolayers of the CdS shells. When the CdS shell thickness exceeded ten monolayers, the PL QY gradually decreased from >90% (CdSe/11CdS) to ~70% (CdSe/16CdS), and

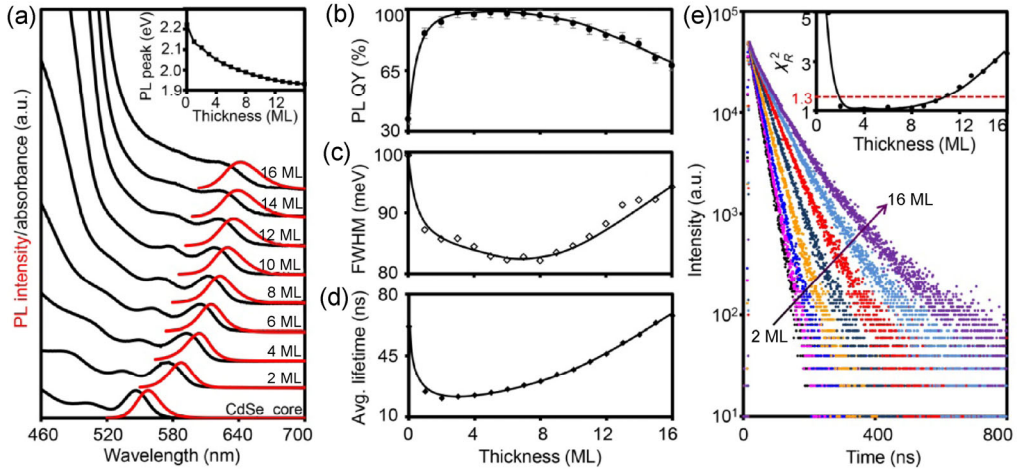

Figure 9 (a) Evolution of UV–Vis and PL spectra during shell growth. Inset: PL peak position vs. the shell thickness. (b) Shell-thickness dependence of PL QY for the reaction shown in (a). (c) Shell-thickness dependence of PL FWHM. (d) Shell-thickness dependence of average PL decay lifetime. (e) Shell-thickness dependence of PL decay curves and goodness-of-fit (χ_R^2) obtained by fitting the PL decay dynamics for each sample to single-exponential function.

the PL decay dynamics deviated slightly from single-exponential (Fig. 9(e)), indicating possible traps caused by late stage epitaxy for the thick-shells. The average PL decay lifetime (Fig. 9(d)) was obtained by fitting the PL decay dynamics for all samples to single-exponential decay dynamics. Given the relatively small deviation from single-exponential decay dynamics (Fig. 9(e), inset), the resulting lifetime values should be meaningful for all core/shell samples.

The shell-thickness dependent trends of the PL QY (Fig. 9(b)), PL FWHM (Fig. 9(c)), average PL decay lifetime (Fig. 9(d)), and χ_R^2 from single-exponential fitting (Fig. 9(e), inset) were found to be reproducible. The PL QY and χ_R^2 exhibited a plateau for samples with between two and ten monolayers of CdS shells, and the two trends approximately mirrored each other. These observations appear to be reasonable because both the PL QY and χ_R^2 reflect the tendency for radiative decay of the excitons.

The average PL decay lifetime increased monotonically for samples with two to sixteen monolayers of the CdSe shells (Fig. 9(d)). This increase in the PL decay lifetime with shell growth appears reasonable. The PL decay lifetime is determined by the overlapping of the electron and hole wavefunctions. For CdSe/CdS core/shell quantum dots, the hole wavefunction should be mostly localized in the core and insensitive to the shell thickness, whereas the electron wavefunction should be largely delocalized into the CdS shells [47].

The PL FWHM decreased monotonically in moving from the core to eight monolayers of the CdS shells and increased when the shell thickness exceeded eight monolayers of the CdS shells (Fig. 9(c)). The decrease of the PL FWHM upon shell growth followed opposite trends to previous literature reports [48, 49], and further investigation is required to understand this reproducible trend.

Overall, the unique and shell-thickness dependent optical properties described in the above subsections were exceptional in comparison to that of the CdSe/CdS core/shell nanocrystals with the wurtzite structure having similar shell-thicknesses [29, 37]. However, it is still too early to claim that zinc-blende CdSe/CdS core/shell nanocrystals are better than their wurtzite counterparts because the synthetic scheme and the products described herein are of significantly higher structural quality than those of the wurtzite counterparts. For instance, the typical reaction described in the Experimental section is nearly quantitatively reproducible for each monolayer of growth, with 1 nm variation for the PL peak position, which is close to the instrumental resolution (~0.5 nm) for the PL FWHM, ± 3% for the PL QY (systematic error of the measurements), <1 ns for the PL lifetime, and no identifiable diffraction signature of the wurtzite structure. In comparison, synthesis of wurtzite CdSe/

CdS core/shell nanocrystals with similar shell-thicknesses is much less advanced.

3 Conclusion

By setting "zinc-blende CdSe/CdS core/shell nanocrystals with sixteen monolayers of CdS shell" as the synthetic target, several key parameters for epitaxial growth of the core/shell nanocrystals were identified. These key parameters became significantly more important in the synthesis of thick-shell core/shell dots than in growth of thin-shell counterparts. The synthetic chemistry of colloidal nanocrystals was previously compared with total synthesis via organic chemistry [5]. This work, to a certain extent, verified the previous hypothesis. By setting a complex nanocrystal as the synthetic target, the synthesis protocol developed herein may very likely result in the discovery of new chemical insights related to the relevant crystallization processes.

4 Experimental

4.1 Chemicals

Stearic acid (HSt, 90+%), cadmium oxide (CdO, 99.998%), tetramethylammonium hydroxide (98%), octylamine (98%), selenium powder (Se, 200 mesh, 99.999%), 1-octadecence (ODE, 90%), dodecane (99%), and HOl (90%) were purchased from Alfa Aesar. Tributylphosphine (TBP) was purchased from Shanghai Titan Chemicals. Cadmium acetate dihydrate ($CdAc_2{\cdot}2H_2O$, 98.5%) was purchased from Shanghai Tingxin Reagents. Sodium diethyldithiocarbamate trihydrate ($NaDDTC{\cdot}3H_2O$, 99%) was purchased from Aladdin Reagents. Oleylamine (C_{18} content: 80%–90%) was purchased from Acros. All organic solvents were purchased from Sinopharm Reagents. All chemicals were used directly without any further purification unless otherwise stated.

4.2 Synthesis of $CdSt_2$

In a typical synthesis, HSt (20 mmol) was neutralized with tetramethylammonium hydroxide (20 mmol) in methanol (200 mL) by stirring. $CdAc_2{\cdot}2H_2O$ (10 mmol) dissolved in methanol (50 mL) was added dropwise to this solution under vigorous stirring. The formation of white precipitates indicated the formation of $CdSt_2$, and the mixture was stirred for 20 min after finishing the dropping process to ensure complete reaction. Subsequently, the precipitate was collected by filtration, washed thrice with methanol, and then dried under vacuum at room temperature overnight before use.

4.3 Synthesis of $Cd(DDTC)_2$

$Cd(Ac_2){\cdot}2H_2O$ (10 mmol) was dissolved in distilled water (100 mL). NaDDTC (20 mmol) dissolved in distilled water (60 mL) was added dropwise to this solution under vigorous stirring; white precipitates of $Cd(DDTC)_2$ immediately formed. After addition of the NaDDTC solution, the mixture was stirred for 20 min to ensure complete reaction. The precipitate was washed thrice with distilled water and dried under vacuum at room temperature overnight before use.

4.4 Preparation of $Cd(Ol)_2$ solution ($Cd(Ol)_2$:Hol = 1:2)

CdO (0.1284 g, 1 mmol), HOl (1.1299 g, 4 mmol), and ODE (6.8917 g) were mixed in a 25 mL flask. After stirring and bubbling with argon for 10 min, the flask was heated to 240 ℃ to obtain a clear solution.

4.5 Preparation of $Cd(Ol)_2$ solution ($Cd(Ol)_2$:Hol = 1:6)

CdO (0.1284 g, 1 mmol), HOl (2.2598 g, 8 mmol), and ODE (5.8934 g) were mixed in a 25 mL flask. After stirring and bubbling with argon for 10 min, the flask was heated to 240 ℃ to obtain a clear solution.

4.6 Synthesis of $Cd(Ol)_2$

CdO (1.2841 g, 10 mmol) and HOl (11.2988 g, 40 mmol) were mixed in a 25 mL flask. After stirring and bubbling with argon for 10 min, the flask was heated to 240 ℃ to obtain a clear solution. The reaction mixture was allowed to cool to 50 ℃ and then slowly poured into acetone (100 mL). White precipitates of $Cd(Ol)_2$ immediately formed; the precipitate was collected by filtration, washed thrice with acetone, and dried under vacuum overnight at room temperature before use.

4.7 Synthesis of CdSe core nanocrystals using non-injection method

In a typical synthesis, $Cd(St)_2$ (0.1356 g, 0.2 mmol), Se powder (0.0079 g, 0.1 mmol), and ODE (4 mL) were loaded into a 25 mL three-neck flask. After stirring and bubbling with argon for 10 min, the mixture was heated to 250 ℃. Needle tip aliquots were withdrawn for UV−Vis and PL measurements to monitor the reaction. When the targeted nanocrystal size was achieved, the reaction mixture was allowed to cool to 50 ℃, and the *in situ* purification procedure described below was employed to purify the nanocrystals.

4.8 Synthesis of CdSe nanocrystals using Se-SUS

In a typical synthesis, $CdSt_2$ (0.0256 g, 0.2 mmol) and ODE (3.5 mL) were loaded into a 25 mL three-neck flask. After stirring and bubbling with argon for 10 min, the mixture was heated to 250 ℃. Se-SUS was prepared by dispersing Se powder (0.0237 g, 0.30 mmol) in ODE (3 mL) by sonication for 5 min. A 0.6 mL aliquot of 0.1 mol·L^{-1} Se-SUS was quickly injected into the reaction flask at 250 ℃. The reaction temperature was maintained at 250 ℃ for further growth. After growth for 8 min, another shot of 0.1 mol·L^{-1} Se-SUS (0.1 mL) was injected into the reaction solution. About 3–4 min later, a third aliquot (0.05 mL) of Se-SUS was injected. Multiple injections were performed at intervals of 3–4 min using 0.05 mL of Se-SUS until the size of the nanocrystals reached 3.0 nm. Needle-tip aliquots were withdrawn and dissolved in toluene for UV−Vis and PL measurements to monitor the reaction. When the targeted size of the nanocrystals was achieved, the reaction mixture was allowed to cool to 50 ℃, and the *in situ* purification procedure described below was employed to purify the nanocrystals.

4.9 *In situ* purification procedure for core nanocrystals

An *in situ* purification procedure was employed to purify the CdSe core nanocrystals. TBP (0.2 mL), octylamine (0.2 mL), hexane (4 mL), and methanol (8 mL) were added to the reaction solution at 50 ℃ and stirred for 2 min. The ODE/hexane layer and methanol layer were separated after stirring was discontinued; the lower colorless methanol layer was withdrawn with a syringe to remove the unreacted precursors and side products. This extraction procedure was repeated four times, but TBP and octylamine were only added in the first and third steps. The hexane and trace amounts of methanol left in the flask were removed by bubbling with argon at about 60 ℃.

4.10 Preparation of precursor solution for shell growth

The single-source precursor solution (0.1 mol·L^{-1}) was prepared by dissolving $Cd(DDTC)_2$ (0.4089 g, 1 mmol) in a mixture of dodecane (7.5 mL) and oleylamine (2.5 mL). The $Cd(Ol)_2$ solution (0.1 mol·L^{-1}) was prepared by dissolving $Cd(Ol)_2$ (0.6773 g, 1 mmol) in a mixture of oleylamine (0.5349 g, 2 mmol) and ODE (7.3689 g).

4.11 Synthesis of CdSe/CdS core/shell nanocrystals

In a typical synthesis, dodecane (3.8 mL), octylamine (1.05 mL), oleylamine (0.45 mL), and about 0.7 mL of purified CdSe core solution (containing about 2×10^{-7} mol of nanocrystals) were added to a three-neck flask under argon flow, and the mixture was heated to 80 ℃. The amount of precursor solution for each injection was estimated based on the extinction coefficients [50] and calibrated against the TEM measurements. For example, for the reaction with 2×10^{-7} mol of 3.0 nm CdSe core, the amount of $Cd(DDTC)_2$-amine solution required for six consecutive injections was calibrated as 0.08, 0.11, 0.15, 0.20, 0.26, and 0.32 mL, respectively. After injecting the first aliquot of $Cd(DDTC)_2$ precursor solution into this reaction flask, the reaction solution was heated to 160 ℃ in 5 min and kept for another 20 min. The reaction mixture was then allowed to cool to 80 ℃; for growth of the next five monolayers of CdS, the reaction cycle was the same as that used for the first monolayer, except that the growth temperature was 150 ℃. From the seventh monolayer of CdS, precursor solutions (50% of $Cd(DDTC)_2$ and 50% of $Cd(Ol)_2$) in the calibrated volumes for each monolayer were injected, and the temperature was set at 160 ℃. The calibrated volumes for growth of 7 to 16 monolayers of the CdS shell were 0.39, 0.46, 0.54, 0.63, 0.72, 0.82, 0.93, 1.04, 1.16, and 1.29 mL, respectively, each of which included both $Cd(DDTC)_2$ and $Cd(Ol)_2$.

4.12 Optical measurements

UV−Vis spectra were acquired with an Analytik Jena S600 UV−Visible spectrophotometer. Photoluminescence spectra were recorded using an Edinburgh Instrument, FLS920. The absolute PL QY was measured on an integrating sphere coupled with a QE65000 spectrometer from Ocean Optical Co., Ltd. The nanocrystal sample was diluted to gradient values of the optical density by using toluene, and multiple measurements were performed for each sample after the diluted solutions were equilibrated at room temperature.

4.13 TEM and HRTEM

Low-resolution TEM images were acquired with a Hitachi 7700 transmission electron microscope using an acceleration voltage of 80 kV and copper grids (400-mesh) coated with pure carbon support film. HRTEM images were acquired with a JEOL JEM-2100 microscope at an acceleration voltage of 200 kV using copper grids coated with ultrathin carbon film. The toluene solution containing nanocrystals was deposited on the carbon film on copper grids.

4.14 XRD

XRD patterns were obtained using a Rigaku Ultimate-IV X-ray diffractometer operating at 40 kV/40 mA using the Cu-Kα line (λ = 1.5418 Å). Powder samples for XRD measurements were prepared by precipitation of the nanocrystals from the solution to ensure acquisition of diffraction patterns with good quality. The nanocrystals were extracted thrice with hexane and methanol (volume ratio = 1:2) and then precipitated using acetone. The precipitate was separated by decantation of the waste solution and transferred onto a glass slide for XRD measurements.

4.15 PL decay dynamics

PL decay curves were acquired with a time-correlated single-photon counting (TCSPC) spectrofluorometer (FL900, Edinburgh Instrument, UK) at room temperature. The nanocrystal samples were diluted in a toluene solution and excited with a 405 nm picosecond laser diode with a repetition rate of 2 MHz. The peak photon count was set at 5,000 for all measurements.

Acknowledgements

The financial support from the National Natural Science Foundation of China (Nos. 21233005 and 91433204) is acknowledged.

Electronic Supplementary Material: Supplementary material (additional TEM and HRTEM images of zinc-blende CdSe/CdS core/shell nanocrystals with thick shell synthesized with different parameter, FWHM and PL spectra of zinc-blende CdSe/CdS core/shell nanocrystals synthesized with different amine) is available in the online version of this article at http://dx.doi.org/10.1007/s12274-016-1287-3.

References

[1] Murray, C. B.; Kagan, C. R.; Bawendi, M. G. Synthesis and characterization of monodisperse nanocrystals and close-packed nanocrystal assemblies. *Annu. Rev. Mater. Sci.* **2000**, *30*, 545–610.

[2] Peng, X. G. An essay on synthetic chemistry of colloidal nanocrystals. *Nano Res.* **2009**, *2*, 425–447.

[3] Tamang, S.; Lincheneau, C.; Hermans, Y.; Jeong, S.; Reiss, P. Chemistry of InP nanocrystal syntheses. *Chem. Mater.* **2016**, *28*, 2491–2506.

[4] Cozzoli, P. D.; Pellegrino, T.; Manna, L. Synthesis, properties and perspectives of hybrid nanocrystal structures. *Chem. Soc. Rev.* **2006**, *35*, 1195–1208.

[5] Peng, X. G. Band gap and composition engineering on a nanocrystal (BCEN) in solution. *Acc. Chem. Res.* **2010**, *43*, 1387–1395.

[6] de Mello Donegá, C. Synthesis and properties of colloidal heteronanocrystals. *Chem. Soc. Rev.* **2011**, *40*, 1512–1546.

[7] Bouet, C.; Tessier, M. D.; Ithurria, S.; Mahler, B.; Nadal, B.; Dubertret, B. Flat colloidal semiconductor nanoplatelets. *Chem. Mater.* **2013**, *25*, 1262–1271.

[8] Hines, M. A.; Guyot-Sionnest, P. Synthesis and characterization of strongly luminescing ZnS-capped CdSe nanocrystals. *J. Phys. Chem.* **1996**, *100*, 468–471.

[9] Peng, X. G.; Schlamp, M. C.; Kadavanich, A. V.; Alivisatos, A. P. Epitaxial growth of highly luminescent CdSe/CdS core/shell nanocrystals with photostability and electronic accessibility. *J. Am. Chem. Soc.* **1997**, *119*, 7019–7029.

[10] Dabbousi, B. O.; Rodriguez-Viejo, J.; Mikulec, F. V.; Heine, J. R.; Mattoussi, H.; Ober, R.; Jensen, K. F.; Bawendi, M. G. (CdSe)ZnS core−shell quantum dots: Synthesis and characterization of a size series of highly luminescent

nanocrystallites. *J. Phys. Chem. B* **1997**, *101*, 9463–9475.

[11] Li, J. J.; Wang, Y. A.; Guo, W. Z.; Keay, J. C.; Mishima, T. D.; Johnson, M. B.; Peng, X. G. Large-scale synthesis of nearly monodisperse CdSe/CdS core/shell nanocrystals using air-stable reagents via successive ion layer adsorption and reaction. *J. Am. Chem. Soc.* **2003**, *125*, 12567–12575.

[12] Xie, R. G.; Kolb, U.; Li, J. X.; Basché, T.; Mews, A. Synthesis and characterization of highly luminescent CdSe–core CdS/$Zn_{0.5}Cd_{0.5}$S/ZnS multishell nanocrystals. *J. Am. Chem. Soc.* **2005**, *127*, 7480–7488.

[13] Nan, W. N.; Niu, Y. A.; Qin, H. Y.; Cui, F.; Yang, Y.; Lai, R. C.; Lin, W. Z.; Peng, X. G. Crystal structure control of zinc-blende CdSe/CdS core/shell nanocrystals: Synthesis and structure-dependent optical properties. *J. Am. Chem. Soc.* **2012**, *134*, 19685–19693.

[14] Chen, O.; Zhao, J.; Chauhan, V. P.; Cui, J.; Wong, C.; Harris, D. K.; Wei, H.; Han, H. S.; Fukumura, D.; Jain, R. K. et al. Compact high-quality CdSe–CdS core–shell nanocrystals with narrow emission linewidths and suppressed blinking. *Nat. Mater.* **2013**, *12*, 445–451.

[15] Gao, Y.; Peng, X. G. Photogenerated excitons in plain core CdSe nanocrystals with unity radiative decay in single channel: The effects of surface and ligands. *J. Am. Chem. Soc.* **2015**, *137*, 4230–4235.

[16] Chen, Y. F.; Vela, J.; Htoon, H.; Casson, J. L.; Werder, D. J.; Bussian, D. A.; Klimov, V. I.; Hollingsworth, J. A. "giant" multishell CdSe nanocrystal quantum dots with suppressed blinking. *J. Am. Chem. Soc.* **2008**, *130*, 5026–5027.

[17] Mahler, B.; Spinicelli, P.; Buil, S.; Quelin, X.; Hermier, J. P.; Dubertret, B. Towards non-blinking colloidal quantum dots. *Nat. Mater.* **2008**, *7*, 659–664.

[18] Greytak, A. B.; Allen, P. M.; Liu, W. H.; Zhao, J.; Young, E. R.; Popović, Z.; Walker, B. J.; Nocera, D. G.; Bawendi, M. G. Alternating layer addition approach to CdSe/CdS core/shell quantum dots with near-unity quantum yield and high on-time fractions. *Chem. Sci.* **2012**, *3*, 2028–2034.

[19] Nirmal, M.; Dabbousi, B. O.; Bawendi, M. G.; Macklin, J. J.; Trautman, J. K.; Harris, T. D.; Brus, L. E. Fluorescence intermittency in single cadmium selenide nanocrystals. *Nature* **1996**, *383*, 802–804.

[20] Murayama, M.; Nakayama, T. Chemical trend of band offsets at wurtzite/zinc-blende heterocrystalline semiconductor interfaces. *Phys. Rev. B* **1994**, *49*, 4710–4724.

[21] Bandić, Z. Z.; Ikonić, Z. Electronic structure of (Zn,Cd)(S,Se)-based polytype superlattices. *Phys. Rev. B* **1995**, *51*, 9806–9812.

[22] Efros, A. L.; Rosen, M.; Kuno, M.; Nirmal, M.; Norris, D. J.; Bawendi, M. Band-edge exciton in quantum dots of semiconductors with a degenerate valence band: Dark and bright exciton states. *Phys. Rev. B* **1996**, *54*, 4843–4856.

[23] Galland, C.; Brovelli, S.; Bae, W. K.; Padilha, L. A.; Meinardi, F.; Klimov, V. I. Dynamic hole blockade yields two-color quantum and classical light from dot-in-bulk nanocrystals. *Nano Lett.* **2013**, *13*, 321–328.

[24] Mahler, B.; Lequeux, N.; Dubertret, B. Ligand-controlled polytypism of thick-shell CdSe/CdS nanocrystals. *J. Am. Chem. Soc.* **2010**, *132*, 953–959.

[25] Washington, A. L.; Foley, M. E.; Cheong, S.; Quffa, L.; Breshike, C. J.; Watt, J.; Tilley, R. D.; Strouse, G. F. Ostwald's rule of stages and its role in cdse quantum dot crystallization. *J. Am. Chem. Soc.* **2012**, *134*, 17046–17052.

[26] Gao, Y.; Peng, X. G. Crystal structure control of CdSe nanocrystals in growth and nucleation: Dominating effects of surface versus interior structure. *J. Am. Chem. Soc.* **2014**, *136*, 6724–6732.

[27] Qin, H. Y.; Niu, Y.; Meng, R. Y.; Lin, X.; Lai, R. C.; Fang, W.; Peng, X. G. Single-dot spectroscopy of zinc-blende CdSe/CdS core/shell nanocrystals: Nonblinking and correlation with ensemble measurements. *J. Am. Chem. Soc.* **2014**, *136*, 179–187.

[28] Dai, X. L.; Zhang, Z. X.; Jin, Y. Z.; Niu, Y.; Cao, H. J.; Liang, X. Y.; Chen, L. W.; Wang, J. P.; Peng, X. G. Solution-processed, high-performance light-emitting diodes based on quantum dots. *Nature* **2014**, *515*, 96–99.

[29] Ghosh, Y.; Mangum, B. D.; Casson, J. L.; Williams, D. J.; Htoon, H.; Hollingsworth, J. A. New insights into the complexities of shell growth and the strong influence of particle volume in nonblinking "giant" core/shell nanocrystal quantum dots. *J. Am. Chem. Soc.* **2012**, *134*, 9634–9643.

[30] Jung, Y. K.; Kim, J. I.; Lee, J. K. Thermal decomposition mechanism of single-molecule precursors forming metal sulfide nanoparticles. *J. Am. Chem. Soc.* **2010**, *132*, 178–184.

[31] Pu, C. D.; Peng, X. G. To battle surface traps on CdSe/CdS core/shell nanocrystals: shell isolation versus surface treatment. *J. Am. Chem. Soc.* **2016**, *138*, 8134–8142.

[32] Protière, M.; Reiss, P. Facile synthesis of monodisperse ZnS capped CdS nanocrystals exhibiting efficient blue emission. *Nanoscale Res. Lett.* **2006**, *1*, 62–67.

[33] Chen, D. A.; Zhao, F.; Qi, H.; Rutherford, M.; Peng, X. G. Bright and stable purple/blue emitting CdS/ZnS core/shell nanocrystals grown by thermal cycling using a single-source precursor. *Chem. Mater.* **2010**, *22*, 1437–1444.

[34] Yang, Y.; Qin, H. Y.; Peng, X. G. Intramolecular entropy and size-dependent solution properties of nanocrystal–ligands complexes. *Nano Lett.* **2016**, *16*, 2127–2132.

[35] Yang, Y.; Qin, H. Y.; Jiang, M. W.; Lin, L.; Fu, T.; Dai, X. L.; Zhang, Z. X.; Niu, Y.; Cao, H. J.; Jin, Y. Z. et al. Entropic ligands for nanocrystals: From unexpected solution properties

to outstanding processability. *Nano Lett.* **2016**, *16*, 2133–2138.

[36] Tan, R.; Blom, D. A.; Ma, S. G.; Greytak, A. B. Probing surface saturation conditions in alternating layer growth of CdSe/CdS core/shell quantum dots. *Chem. Mater.* **2013**, *25*, 3724–3736.

[37] Guo, Y. J.; Marchuk, K.; Sampat, S.; Abraham, R.; Fang, N.; Malko, A. V.; Vela, J. Unique challenges accompany thick-shell CdSe/*n*CdS (n > 10) nanocrystal synthesis. *J. Phys. Chem. C* **2012**, *116*, 2791–2800.

[38] Thessing, J.; Qian, J. H.; Chen, H. Y.; Pradhan, N.; Peng, X. G. Interparticle influence on size/size distribution evolution of nanocrystals. *J. Am. Chem. Soc.* **2007**, *129*, 2736–2737.

[39] Talapin, D. V.; Nelson, J. H.; Shevchenko, E. V.; Aloni, S.; Sadtler, B.; Alivisatos, A. P. Seeded growth of highly luminescent CdSe/CdS nanoheterostructures with rod and tetrapod morphologies. *Nano Lett.* **2007**, *7*, 2951–2959.

[40] Ji, X. H.; Copenhaver, D.; Sichmeller, C.; Peng, X. G. Ligand bonding and dynamics on colloidal nanocrystals at room temperature: The case of alkylamines on CdSe nanocrystals. *J. Am. Chem. Soc.* **2008**, *130*, 5726–5735.

[41] Yu, W. W.; Peng, X. G. Formation of high-quality CdS and other II–VI semiconductor nanocrystals in noncoordinating solvents: Tunable reactivity of monomers. *Angew. Chem., Int. Ed.* **2002**, *41*, 2368–2371.

[42] Anderson, N. C.; Hendricks, M. P.; Choi, J. J.; Owen, J. S. Ligand exchange and the stoichiometry of metal chalcogenide nanocrystals: Spectroscopic observation of facile metal-carboxylate displacement and binding. *J. Am. Chem. Soc.* **2013**, *135*, 18536–18548.

[43] Dirksen, A.; Nieuwenhuizen, P. J.; Hoogenraad, M.; Haasnoot, J. G.; Reedijk, J. New mechanism for the reaction of amines with zinc dithiocarbamates. *J Appl. Polym. Sci.* **2001**, *79*, 1074–1083.

[44] van Embden, J.; Jasieniak, J.; Mulvaney, P. Mapping the optical properties of CdSe/CdS heterostructure nanocrystals: The effects of core size and shell thickness. *J. Am. Chem. Soc.* **2009**, *131*, 14299–14309.

[45] Yang, Y. A.; Wu, H. M.; Williams, K. R.; Cao, Y. C. Synthesis of CdSe and CdTe nanocrystals without precursor injection. *Angew. Chem., Int. Ed.* **2005**, *44*, 6712–6715.

[46] Pu, C. D.; Zhou, J. H.; Lai, R. C.; Niu, Y.; Nan, W. N.; Peng, X. G. Highly reactive, flexible yet green Se precursor for metal selenide nanocrystals: Se-octadecene suspension (Se-SUS). *Nano Res.* **2013**, *6*, 652–670.

[47] Brovelli, S.; Schaller, R. D.; Crooker, S. A.; García-Santamaría, F.; Chen, Y.; Viswanatha, R.; Hollingsworth, J. A.; Htoon, H.; Klimov, V. I. Nano-engineered electron–hole exchange interaction controls exciton dynamics in core–shell semiconductor nanocrystals. *Nat. Commun.* **2011**, *2*, 280.

[48] Cui, J.; Beyler, A. P.; Marshall, L. F.; Chen, O.; Harris, D. K.; Wanger, D. D.; Brokmann, X.; Bawendi, M. G. Direct probe of spectral inhomogeneity reveals synthetic tunability of single-nanocrystal spectral linewidths. *Nat. Chem.* **2013**, *5*, 602–606.

[49] Cui, J.; Beyler, A. P.; Coropceanu, I.; Cleary, L.; Avila, T. R.; Chen, Y.; Cordero, J. M.; Heathcote, S. L.; Harris, D. K.; Chen, O. et al. Evolution of the single-nanocrystal photoluminescence linewidth with size and shell: Implications for exciton–phonon coupling and the optimization of spectral linewidths. *Nano Lett.* **2016**, *16*, 289–296.

[50] Yu, W. W.; Qu, L. H.; Guo, W. Z.; Peng, X. G. Experimental determination of the extinction coefficient of CdTe, CdSe, and CdS nanocrystals. *Chem. Mater.* **2003**, *15*, 2854–2860.